Direct Numerical Simulation and RANS Comparison of Turbulent Convective Heat Transfer in a Staggered Ribbed Channel With High Blockage

Luca Marocco[1], Andrea Franco

Department of Energy, Politecnico di Milano, Milan 20156, Italy

A turbulent convective flow of an incompressible fluid inside a staggered ribbed channel with high blockage at ReH 4200 is simulated with direct numerical simulation (DNS) and Reynolds-averaged Navier–Stokes (RANS) techniques. The DNS results provide the reference solution for comparison of the RANS turbulence models. The k–e realizable, k–x SST, and v2 –f model are accurately analyzed for their strengths and weaknesses in predicting the flow and temperature field for this geometry. These three models have been extensively used in literature to simulate this configuration and boundary conditions but with discordant conclusions upon their performance. The v2 –f model performs much bet-ter than the k–e realizable while the k–x SST model results to be inadequate.

1 Introduction

Turbulence promoters in form of ribs are commonly used in various equipment such as turbine cooling channels, heat exchangers, nuclear reactors, and solar air heaters. These artificial roughness surfaces modify the fluid dynamics by various mechanisms, such as periodic interruption of the boundary layer growth or periodic streamline deflection. In addition, they promote turbulence development as their characteristic size is close to the turbulent microscales (the lower the Reynolds number, the larger the size of dissipative structures). Several authors have already tackled this problem, both numerically as well as experimentally. Only the most important literature references related to the present analysis will be here briefly reviewed, in order to justify the necessity of the present study. Among the experimental works, those of Casarsa and Arts [1] and Rau et al. [2] are worth mentioning. The first uses a particle image velocimetry technique to characterize the flow field of air at $Re = 40{,}000$, based on the inlet bulk velocity and hydraulic diameter, in a stationary straight channel with high blockage ribs installed on one wall, thus improving a previous aerothermal analysis made by Çakan [3]. A systematic study by varying the pitch-to-height ratio (p/e) gave the highest value of the global Nusselt number for $p/e = 10$. The latter ratio has then been chosen for the present study.

Several works can be found in the literature dealing with numerical simulations of the flow and thermal field inside a ribbed channel, but still today, there is no agreement on the best performing turbulence model for this type of geometry. Indeed, the sudden flow separation upstream of the rib with subsequent downstream reattachment and the imposed heat flux at the wall represent a challenging task for every RANS model using either wall functions or a low-Re approach.

Recently, Keshmiri [4] compared the flow and heat transfer from RANS simulations on a 3D and 2D ribbed channel with the experimental data of Rau et al. [2]. He concluded that the results on the centerplane can be represented by a 2D simulation with relatively good accuracy, allowing significant savings in computational power and time.

Realistic results of heat transfer performance have been obtained by Iacovides and Raisee [5] and Raisee et al. [6] using a low Reynolds number (LRN) k–ε model with the length-scale correction term to the dissipation rate of Yap [7]. Ooi et al. [8] found that the $\overline{v^2}$–f model gives the closest heat transfer predictions to the experiments compared to the Spalart–Allmaras and the two-layer k–ε model. Chaube et al. [9] compared the heat transfer prediction in the inter-rib region with the experimental results of Tanda [10]. They tested the k–ε realizable, k–ε RNG, standard k–ω, and k–ω SST models, with this last giving the best results. Wongcharee et al. [11] compared the numerical results obtained with the k–ε RNG and k–ω SST turbulence models with the experimental data of Kilicaslan and Sarac [12], concluding that the k–ω SST model performs better. Contrarily, Eiamsa-ard and Promvonge [13] numerically simulated the experimental facility of Lorenz et al. [14] using four different turbulence models, i.e., standard k–ε, k–ε RNG, standard k–ω, and k–ω SST. Best agreement was obtained with the standard k–ε and k–ε RNG models. Previously, Luo et al. [15] showed the superiority of the standard k–ε model over the Reynolds stress model (RSM) in the simulation of the turbulent forced convection in a two-dimensional channel with a ribbed surface. Marocco et al. [16] compared the pressure drop and Nusselt number values obtained with the above-mentioned k–ε and k–ω models with their own experimental data [17] at $Re_H = 4180$ (based on channel height and inlet bulk velocity). None of the models correctly reproduced the measured values. Anyway, because only the k–ε realizable model predicted the experimentally observed inter-rib flow reattachment for this p/e ratio, it was judged to be more appropriate to simulate the turbulent convection inside ribbed channels at low Reynolds number values. Subsequently, the same authors [18] again compared the numerical simulations to their experimental data, showing once again the inability of RANS models in correctly predicting heat transfer for this configuration. Their use is then only recommended for qualitative information or to identify the most promising configurations that should be subsequently experimentally and numerically analyzed with large eddy simulation (LES) or DNS techniques. Regarding the last consideration, the interest in low Reynolds number flows through ribbed channels for electronics or

[1]Corresponding author.
e-mail: luca.marocco@polimi.it
Contributed by the Heat Transfer Division of ASME for publication in the Journal of Heat Transfer. Manuscript received May 1, 2016; final manuscript received August 26, 2016; published online October 11, 2016. Assoc. Editor: Jim A. Liburdy.

even turbine blades cooling motivates the use of a DNS for the present work. Although this technique has already been used to analyze the turbulent flow and thermal field inside a channel with artificial roughness [19,20], to the authors' knowledge there is no systematic comparison between DNS and RANS results for this type of geometry, flow, and thermal boundary conditions. According to the above considerations, the RANS simulations are carried out with the three most promising turbulence models, i.e., k–ε realizable, k–ω SST, and $\overline{v^2}$–f.

The commercial finite-volume CFD software FLUENT v13.0 has been used for both RANS and DNS simulations. Its capability to perform the latter for the flow field inside a smooth channel has already been proven by Rossi [21]. Anyway, as pointed out by Arts et al. [22], its limitations in solving the unsteady temperature field with streamwise and spanwise periodic conditions have prevented its use for a direct numerical simulation of the heat transfer. For the present work, a methodology has been developed to fix this problem and correctly solve the unsteady energy equation with FLUENT using biperiodic boundary conditions. Appropriate libraries have been also developed and coupled to the code for the run-time calculations of the statistics and the efficient management of the postprocessing results, thus significantly reducing the computational time. A detailed description of the additional modules developed can be found in Ref. [23].

2 Simulations Setup

2.1 Computational Domain and Governing Equations. A section of the computational domain perpendicular to the z-coordinate is shown in Fig. 1 together with the main dimensions and boundary conditions. Two-dimensional staggered rectangular ribs of the same width and height are positioned on the lower and upper walls. The rib height is 16.7% of the channel height.

The governing equations for a streamwise periodic incompressible Newtonian fluid with constant thermophysical properties and neither gravitational body forces nor viscous dissipation read as follows:

$$\frac{\partial u_i}{\partial x_i} = 0 \tag{1}$$

$$\frac{\partial u_i}{\partial t} + \frac{\partial (u_i u_j)}{\partial x_j} = -\frac{1}{\rho}\frac{\partial \hat{P}}{\partial x_i} + \nu \frac{\partial^2 u_i}{\partial x_j \partial x_j} + \frac{\beta}{\rho}\delta_{i1} \tag{2}$$

$$\frac{\partial \hat{T}}{\partial t} + \frac{\partial \left(u_i \hat{T}\right)}{\partial x_i} = \alpha \frac{\partial^2 \hat{T}}{\partial x_i \partial x_i} - u_i \gamma \delta_{i1} \tag{3}$$

The above Eqs. (1) and (2) are the Navier–Stokes equations, while Eq. (3) is the energy transport equation. $\hat{P}$ and $\hat{T}$ are the periodic components of pressure and temperature [24], while $\beta = \Delta P / L_x$ and $\gamma = \{[q_w(L_z - e)]/(\dot{m} c_p)\}$ can be derived from a force and an energy balance (this last for $q_w = \text{const.}$), respectively.

Periodic boundary conditions for u, $\hat{P}$, and $\hat{T}$ have been imposed in streamwise and spanwise directions. No-slip condition has been enforced at all walls, while the imposed wall heat flux results in the following temperature boundary conditions at the solid surfaces, with $\mathbf{n}$ being the unit normal vector pointing outward from the wall:

$$\frac{\partial \hat{T}}{\partial n} = \begin{cases} 0 & \text{adiabatic wall} \\ \mp\gamma & \text{adiabatic wall and} \quad \mathbf{n} = \pm\nabla x / \|\nabla x\| \\ -q_w/\lambda & \text{heated wall and} \quad \mathbf{n} \perp \nabla x \end{cases} \tag{4}$$

2.2 Numerical Setup DNS. Equations (2) and (3) are solved in a segregated manner using the colocated finite-volume code FLUENT v13.0. Time advancement is performed by a fully implicit second-order accurate scheme. The spatial discretization of the diffusive terms and the values of the velocity components at cell faces are evaluated with a second-order accurate central difference scheme (CDS). The deferred-correction technique is adopted to improve the stability of the advection schemes. The pressure values at cell faces are calculated with a formally second-order multidimensional linear reconstruction approach [25]. This formulation requires the determination of the gradient of the scalar variable in each cell center, accomplished using the so-called *least-squares cell-based gradient evaluation* [26]. The pressure–velocity coupling is performed by the fractional step method (FSM) [27]. This solution methodology applies to the momentum equation. The energy equation (Eq. (3)) is implemented through a user-defined scalar (UDS) equation together with user-defined functions (UDFs) for the boundary conditions and source terms, as thoroughly discussed in Ref. [23]. FLUENT does not allow to use the noniterative time advancement scheme when the scalar equation is solved. Therefore, initially only the flow field is computed using a noniterative time advancement scheme with the FSM for the pressure–velocity coupling. Once a statistically steady flow field is reached, both flow and temperature field are computed using an iterative time advancement scheme with the SIMPLE algorithm for pressure–velocity coupling [28]. The number of internal iterations is set to reach internal convergence at every time-step. The convective term of Eq. (3) is discretized in space with a formally second-order linear upwind (SOU) [25] formulation because the less numerically diffusive, but more numerically unstable, CDS is currently not

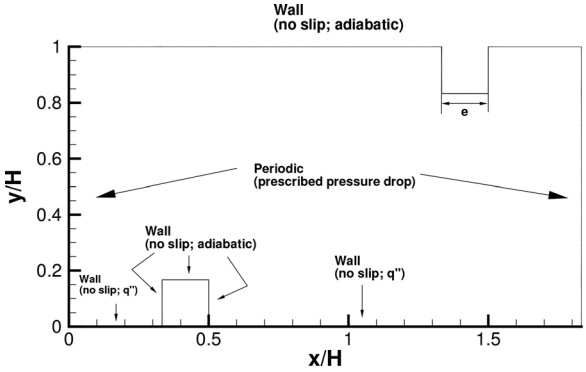

Fig. 1 Computational domain in the *x–y* plane

Table 1 Computational parameters for the DNS of the ribbed channel

Reynolds number	$\mathrm{Re}_H = 4174$
Prandtl number	$\mathrm{Pr} = 0.71$
Computational domain ($L_x \times L_Y \times L_z$)	$1.83H \times H \times 1.6H$
e/H	1/6
p/e	10
Mesh (Δx^+, Δy^+, Δz^+)	$0.2\text{–}2.7 \times 0.002\text{–}0.12 \times 2.9$
No. of elements	3.71×10^6
Coupling algorithm	
Flow	FSM
Flow and energy	SIMPLE
Time advancement	
Flow	Second-order noniterative
Flow and energy	Second-order iterative implicit
Spatial discretization	
Energy; convective terms	SOU
Momentum; nonlinear terms	CDS
Viscous terms	CDS
Boundary conditions	Periodic (x and z directions)
	No-slip (y direction)
	$q_w = \text{const.}$ on bottom wall
	$q_w = 0$ on upper wall and ribs
Computational time-step	$\Delta t = 10^{-5}$ s/$\Delta t^+ = 6 \times 10^{-4}$

available in FLUENT for the scalar transport equation. Table 1 summarizes the parameters used for this simulation.

A Cartesian grid has been used with a finer spacing close to the walls and the ribs, in order to properly resolve the near-wall effects. The first grid point is $0.002H$ away from each surface in all directions. Depending on the local friction velocity, it corresponds to 0.0018–0.12 wall units with a mean value of 0.05, coinciding with that used by Kim et al. [29] for a smooth channel flow. Two different stretching ratios (SR) are used, i.e., $SR_1 = 1.1$ from the bottom wall to the top of the rib and $SR_2 = 1.2$ from the rib top to the center of the channel. A uniform grid is used in the spanwise direction. No other grids were used since this grid was already found adequate for the computations. Indeed, from a two-point correlation analysis, the resulting computational domain of $1.83H \times H \times 1.6H$ has been found appropriate for the simulations. A time-step of $\Delta t = 10^{-5}$ s has been used, corresponding to $\Delta t^+ = 6 \times 10^{-4}$ calculated with the friction velocity of a smooth channel at the same Re_H.

All simulations, both for the plane channel flow as well as for the ribbed duct, are carried out on a distributed cluster of 16 processors Xeon E5620 (2.4 GHz) with a total of 64 GB RAM.

The initial flow and temperature fields for the ribbed channel simulations have been obtained from a previous RANS simulation on a scaled grid with 650,240 cells. In order to obtain a flow with the required Re_H, a trial-and-error procedure has been necessary to determine the correct driving pressure gradient. Mean values have been time and spanwise averaged. After reaching a statistically steady state, time averaging has been performed on 12,000 samples (30 flow passages), corresponding to a computational time of 85 h.

2.3 Numerical Setup RANS. Three different RANS turbulence models available in FLUENT v13.0 have been used for the 2D simulations of the ribbed channel, i.e., the k–ε realizable model [30], the k–ω SST model [31], and the $\overline{v^2}$–f model [32]. While CDS has been used for approximating the convective terms in the momentum and energy equations, an SOU scheme [25] has been used for k, ε, $\overline{v^2}$, and f, because the code does not allow to choose a CDS for these variables. The SIMPLE scheme has been used for the pressure–velocity coupling. While the k–ω SST and $\overline{v^2}$–f are low-Re models and can be therefore integrated all the way down through the viscous sublayer, adaptive wall functions, the so-called *enhanced wall functions* (EWT) [26], have been used for the k–ε realizable model. Here, the domain is subdivided into a viscosity affected region and an outer region. In the first, ε is analytically determined through the one-equation model of Wolfshtein [33], while momentum and k are obtained by solving the corresponding transport equations.

The simulations have been carried out on three different 2D grids with increasing number of finite volumes. In order to limit their number, the domain is asymmetrically meshed using a non-conformal interface along the channel's centerline, thus in a region where the gradients of the variables are low, minimizing the interpolation error. Already with the intermediate mesh grid-independent results have been obtained. The node spacing is uniform in the y direction from the walls until the top of the ribs. Thereafter, it increases with a specified stretching factor until the channel's centerline. Starting from the wall-normal rib surfaces, a stretching factor is also applied in the streamwise direction. The maximum grid size in both directions is limited to a specified maximum value. A y^+ value less than 1 at the first mesh node has been ensured in all simulations. The flow is driven by a constant pressure gradient of the same magnitude as that of the DNS. The computational details of the RANS simulations are summarized in Table 2, where the friction velocity is evaluated from a plane channel flow at $Re_H = 4174$. Because the "standard" energy equation of FLUENT is here solved instead of a user-defined scalar transport equation, it has been possible to use a central-differencing scheme for the temperature as well.

Steady-state simulations have been always done with the k–ε realizable model. Due to slow or difficult convergence, transient unsteady calculations have been sometimes necessary with the k–ω SST and $\overline{v^2}$–f models, especially with the finest grids.

Table 2 Computational parameters for RANS ribbed channel simulations

Prandtl number	$Pr = 0.71$
Computational domain ($L_x \times L_Y$)	$1.83H \times H$
e/H	1/6
p/e	10
Mesh fine; SR = 1.0125	$\Delta x^+ = 0.97$–3.75; $\Delta y^+ = 0.97$–2
Coupling algorithm	SIMPLE
Spatial discretization	
Momentum and energy	CDS
$k, \varepsilon, \overline{v^2}, f$	SOU
Boundary conditions	Periodic (x directions)
	No-slip (walls and ribs)
	q_w = const. on bottom wall
	$q_w = 0$ on upper wall and ribs

3 Results

In what follows, the results from the DNS are considered to be the "exact" reference solution.

Recently, Van Haren [34] successfully performed simulations of the temperature field with imposed heat flux at the walls for a turbulent channel and a pipe flow using an open source (OPENFOAM) and a commercial CFD code (STAR-CCM+). In order to test the capability of FLUENT in performing a DNS of the ribbed channel, a numerical simulation of the forced convection inside a smooth channel at $Re_\tau = 180$ has been first carried out. The results have been compared with the available datasets of Kim et al. [29], which use a spectral difference method, and Kawamura [35], which use a high-order finite difference method. The results of this comparison are not reported here but can be found in Ref. [23]. The calculated values of mean velocity and temperature, root-mean-square (RMS) of velocity and temperature fluctuations, the Reynolds stresses and turbulent heat fluxes, as well as the budget of turbulent kinetic energy show good agreement with the DNS data.

As already experimentally observed by Wang et al. [36] and numerically simulated with the LES technique by Lohász et al. [37] and Cui et al. [38], four recirculating regions can be distinguished. The most relevant one is the large bubble downstream of the rib. A secondary bubble, the only one rotating counterclockwise, is formed in the corner downstream of the rib as the reverse flow approaches the vertical surface. Upstream of the rib, another separation bubble occurs as a result of the strong adverse pressure gradient. Moreover, a separated region also creates on the top of the obstacle. Of course, the same structures also appear near the top side rib and wall. The flow separates and reattaches within the grooves between two consecutive ribs. Moreover, the ribs alter the flow over the entire channel's section, as can be seen by the deflected streamlines.

The flow field obtained with the RANS models is compared in Fig. 2 with that of the DNS. The absence of a reattachment at the top of the rib is correctly reproduced by all models. The major differences are found downstream of the obstacles. Indeed, the k–ω SST model strongly overpredicts the streamwise extension of the big recirculation zone, while it underpredicts the latter in the wall-normal direction. Also the $\overline{v^2}$–f model clearly estimates a reattachment point beyond that of the DNS. The topology of this vortex region is best reproduced by the k–ε realizable model. The size of the counter-rotating bubble downstream of the ribs is quite well approximated except by the k–ω SST model, which once again predicts a much larger recirculating region.

Because the flow is driven by an imposed pressure gradient, these dissimilarities in the flow topology lead to differences in the

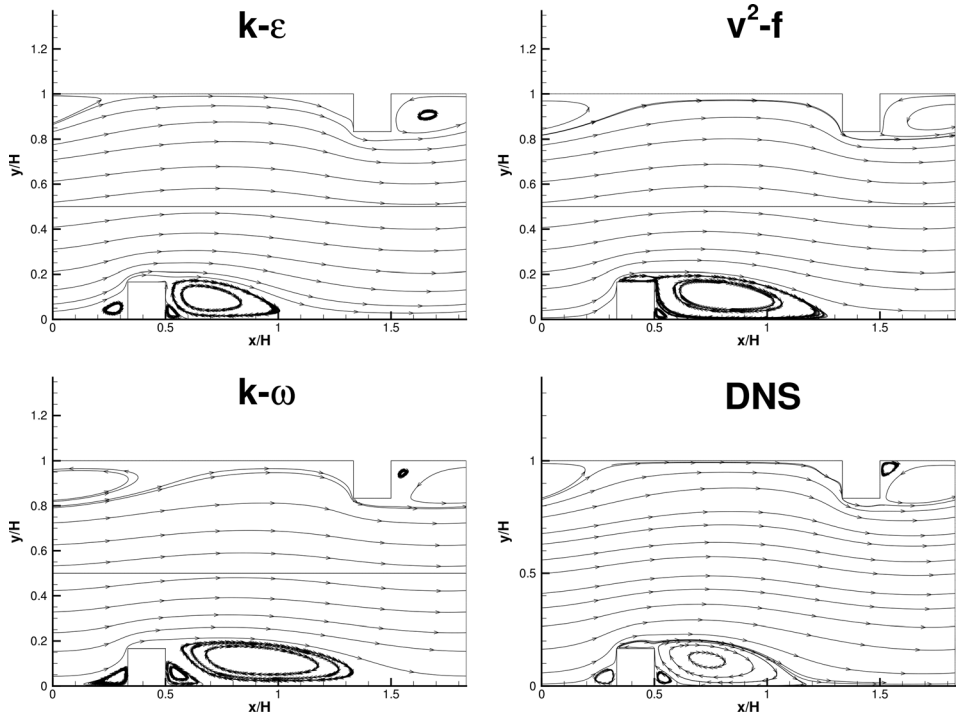

Fig. 2 Streamlines comparison between RANS and DNS

mean inlet bulk velocities, and thus in Re_H, as listed in Table 3, which also summarizes the separation points upstream of the rib, on the rib itself, and the downstream reattachment location. Only the $\overline{v^2}$–f model returns the same u_b as the DNS, while the k–ε realizable and especially the k–ω SST model predict a higher value, and thus a higher mass flow rate for the imposed pressure gradient.

Figure 3 compares the RANS streamwise velocity profiles with those from the DNS computation at different positions downstream and upstream of the ribs. The different turbulence models predict the same trends, in accordance with the DNS ones. Nevertheless, the k–ω SST model markedly shows different magnitudes of streamwise velocity, which reflect in the different value of the mean bulk velocity. Close to the separation/reattachment points at the walls, the streamwise velocity profiles from the RANS simulations show opposite signs from the DNS, according to the over- or underpredicted recirculating bubble.

In the following discussion of the flow field, the k–ω SST model is not considered anymore due to its poor performances, as previously explained.

The profiles of the turbulent kinetic energy are shown in Fig. 4(*a*). The $\overline{v^2}$–f model tends to overpredict it over the entire channel height while the k–ε realizable only in the core region, returning lower values close to the walls. The only exception is found just downstream of the ribs.

The profiles of the wall-normal Reynolds shear stresses are shown in Fig. 4(*b*), where for the RANS models, they are evaluated with the following equation according to the model-dependent turbulent viscosity:

$$-\overline{u'v'} = \nu_t\left(\frac{\partial \overline{u}}{\partial y} + \frac{\partial \overline{v}}{\partial x}\right) \tag{5}$$

Both RANS models underestimate the Reynolds shear stresses close to the walls downstream of the ribs, then gradually recovering the DNS values before slightly overestimating them just upstream of the successive rib. An analogous change between under- and overestimation occurs in the core region. The biggest discrepancies are found at the top of the ribs, especially at the upstream corner, where the models predict turbulent shear stresses of the opposite sign and of much different magnitude. The reason could lie in the value of the eddy diffusivity, always defined positive for the RANS models, failing thus to reproduce the counter-diffusion phenomenon described in Ref. [20]. This last occurs when $-\overline{u'v'}$ and the mean strain rate have opposite signs, owing to negative values of the eddy diffusivity, according to Eq. (5).

Figure 5 shows the comparison of the eddy diffusivity. The k–ε realizable model severely underpredicts ν_t within the shear layer, while the $\overline{v^2}$–f model only in a region closer to the wall up to

Table 3 Comparison of the separation and reattachment points, bulk mean velocities, and Re_H. The distance is expressed in *x*/*H*.

	k–ε real.	$\overline{v^2}$–f	k–ω SST	DNS
Sep.	0	0.16	0.08	0.14
Sep. on rib	0.34	0.34	0.34	0.33
Rea.	1.26	1.33	1.75	1.22
u_b	5.71	5.41	6.16	5.39
Re_H	4420	4188	4769	4174

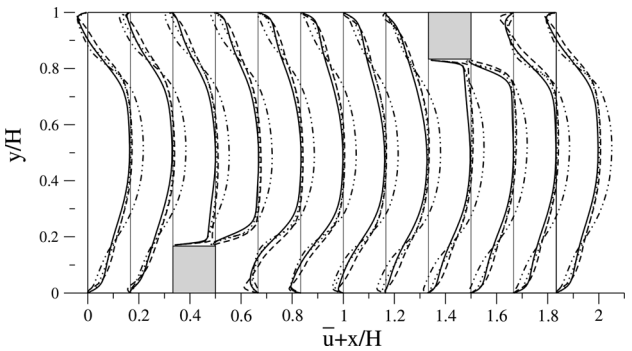

Fig. 3 Comparison of streamwise velocity profiles: DNS (——), k–ε realizable (- - - -), k–ω SST (– - - – - -), and $\overline{v^2}$-f (·····)

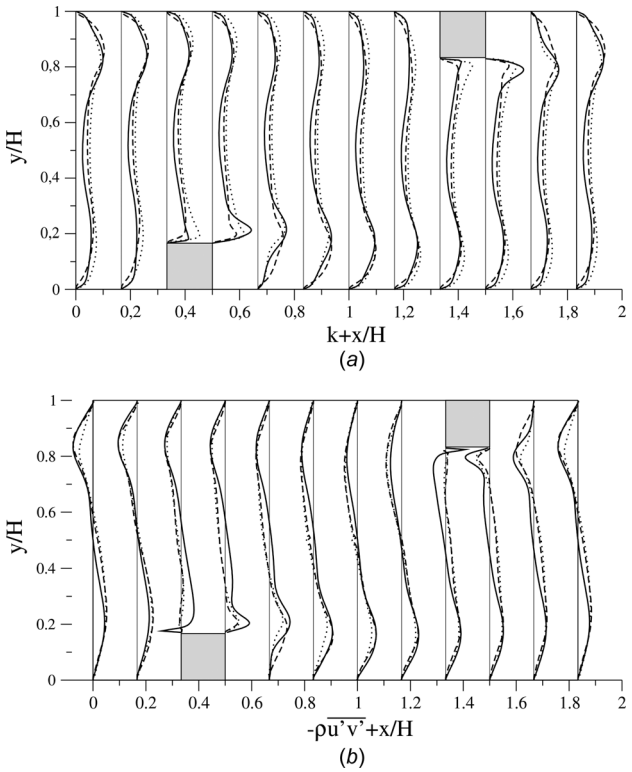

Fig. 4 (*a*) Comparison of turbulent kinetic energy and (*b*) comparison of Reynolds shear stress: DNS (——), *k*–ε realizable (- - - -), and $\overline{v^2}$-*f* (·····)

approximately half of the rib height. Indeed, the $\overline{v^2}$–*f* model is similar to the standard *k*–ε model, but incorporates the near-wall turbulence anisotropy improving its predictions also in separation dominated flows. It can be noted how the turbulent viscosity calculated from the DNS simulations with the Boussinesq hypothesis can assume negative values where the mean shear stress and the turbulent shear stress have opposite signs. Moreover, high values of its magnitude appear outside of the shear layer region, where the velocity gradients tend to zero while the Reynolds shear stresses keep a finite value.

In Fig. 6, the temperature field $T^+ = (\overline{T} - T_{b,\text{in}})/T_{\tau,0}$ is shown, where $T_{\tau,0}$ is evaluated with u_τ of a smooth channel at the same Re_H. The *k*–ε realizable and $\overline{v^2}$–*f* results are in quite good agreement with the DNS away from the shear layer region, while they deteriorate close to the wall resulting in a strongly over- and slightly underprediction of the wall temperature, respectively (Fig. 8(*a*)). The major differences are found with the *k*–ω SST model over the whole channel and especially just downstream of

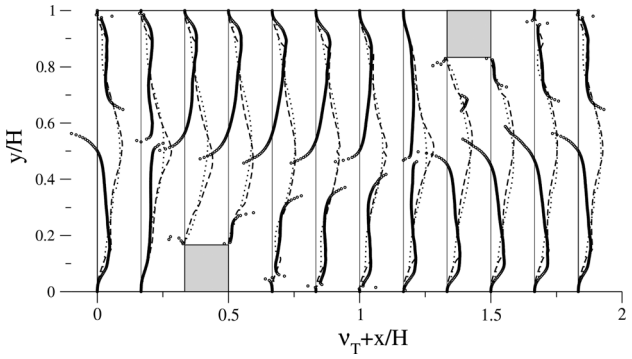

Fig. 5 Comparison of the turbulent momentum diffusivity: DNS (◯), *k*–ε realizable (- - - -), and $\overline{v^2}$-*f* (·····)

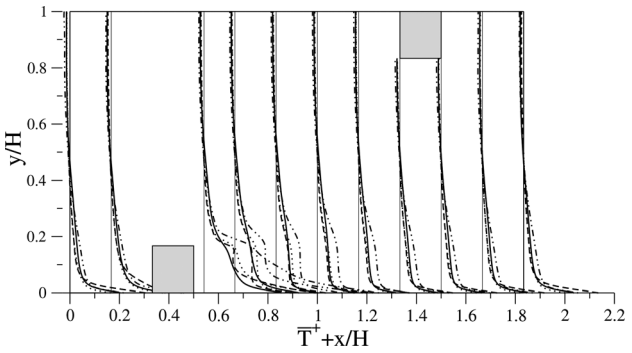

Fig. 6 Comparison of the temperature field: DNS (——), *k*–ε realizable (- - - -), *k*–ω SST (– – – – –), and $\overline{v^2}$-*f* (·····)

the rib, where a very high-temperature value is found, due to the big size of the predicted vortex. When moving away from the wall, the temperature profiles of the RANS models flatten before the ones of the DNS, indicating that the RANS underpredicts the heat turbulent diffusion inside the channel, as shown in Fig. 7 by the normal turbulent heat fluxes. These are computed for the RANS models according to the simple gradient diffusion hypothesis with a constant turbulent Prandtl number $\text{Pr}_t = 0.85$ as follows:

$$\overline{v'T'} = -\alpha_t \frac{\partial \overline{T}}{\partial y} = -\frac{\nu_t}{\text{Pr}_t}\frac{\partial \overline{T}}{\partial y} \tag{6}$$

None of the models correctly predict them, not only in the region close to the rib but also in the groove, where they are underpredicted. Only adjacent to the bottom wall, the $\overline{v^2}$–*f* overpredicts the turbulent heat flux, which is the reason for the lower wall temperature obtained with this model, as shown in Fig. 8(*a*). When moving away from the wall, both RANS models show the same values of $\overline{v'T'}$, even though of lower magnitude than those of the DNS, justifying the steeper temperature profiles in the core region. The reason lies again in the underprediction of the momentum eddy diffusivity, which according to Eq. (6) implies a too low thermal turbulent diffusivity α_t.

Figure 8(*a*) compares the temperature on the heated wall, while Fig. 8(*b*) the ratio between the Nusselt number of the ribbed duct and that of a smooth channel ($\text{Nu}_{H,0}$). The *k*–ω SST model predicts everywhere a too high wall temperature, and thus a too low Nu number, confirming again the inadequacy of this model, as already shown in the discussion of the flow field. The *k*–ε realizable model predicts the same trend as the DNS (i.e., local maxima and minima are located at the same positions), but it overpredicts the wall temperature magnitude, thus underpredicting Nu all along

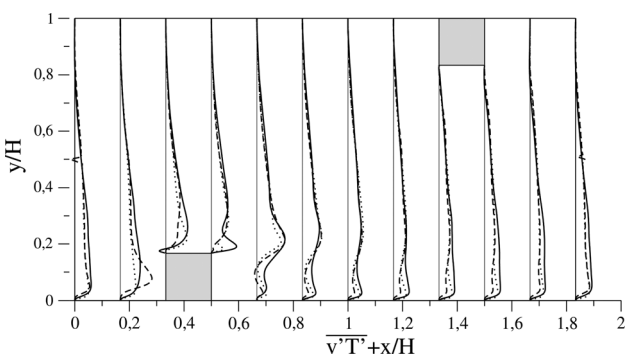

Fig. 7 Comparison of the normal turbulent heat transfer: DNS (——), *k*–ε realizable (- - - -), and $\overline{v^2}$-*f* (·····)

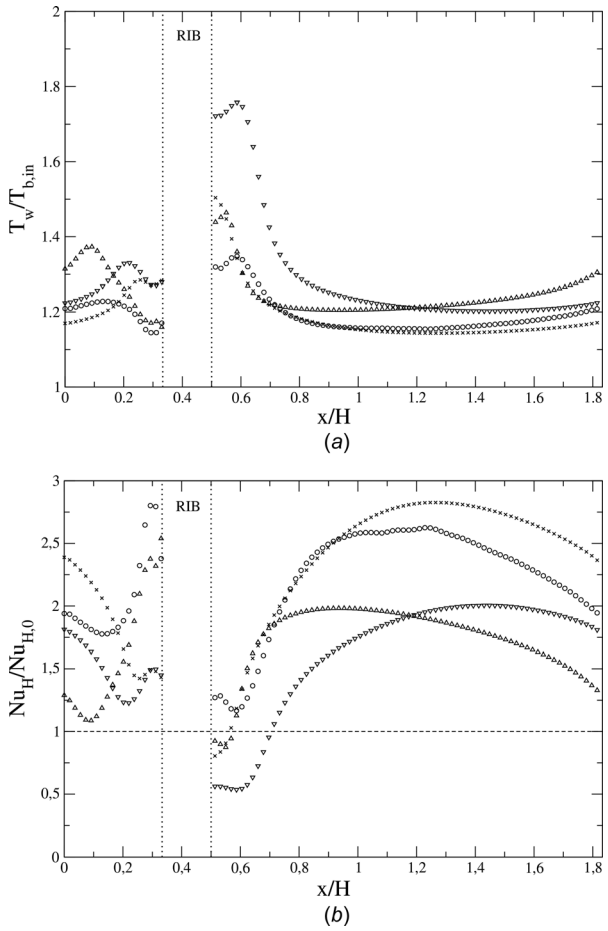

Fig. 8 Wall temperature and Nu number ratio along the bottom wall: (*a*) $T_w/T_{b,\mathrm{in}}$ and (*b*) $\mathrm{Nu}_H/\mathrm{Nu}_{H,0}$; ◯ DNS, △ *k*-ε realizable, ▽ *k*-ω SST, and × $\overline{v^2}$-*f*

the channel, in particular in the groove region. The $\overline{v^2}$–f model instead shows good agreement of T_w and Nu with the DNS in the cavity region between $0.7 < x/H < 1.0$ while it slightly underpredicts T_w over the rest of the wall, except in the regions just upstream and downstream of the ribs, where it severely overpredicts the wall temperature, thus underpredicting Nu.

Finally, Table 4 summarizes the average Nusselt numbers over the entire wall, compared with the measured values from an experimental facility with the same geometry and operating conditions [18]. The results confirm the inadequacy of the k–ε realizable and k–ω SST models, while, due to the averaging procedure, the $\overline{v^2}$–f model predicts a global value in good agreement with the experiment and the DNS. Anyway, as previously discussed, also this model does not correctly predict the local heat transfer.

4 Conclusions

In this work, the turbulent forced convection of an incompressible fluid flowing through a ribbed channel uniformly heated on the bottom wall is investigated through DNS and RANS simulations using the commercial CFD code FLUENT v13.0. The comparison of the results for the flow through a uniformly heated smooth channel with available literature dataset has confirmed the capability of the code to correctly perform a DNS calculation. The DNS has been preferred to the LES because of the low Reynolds number of the flow. Moreover, this choice avoids using a subgrid-scale model close to the solid surfaces, improving then the resolution of the temperature field in the near-wall region. The DNS results have been successively compared with those obtained with three different RANS models, namely, k–ε realizable, k–ω SST, and $\overline{v^2}$–f, that have been extensively used in previous works but with discordant conclusions upon their performance for this geometry configuration and boundary conditions.

The four known recirculating flow structures are predicted by all models but with different extensions, separation, and reattachment points compared to the DNS. In particular, the k–ω SST model shows the worst performances, resulting in markedly different velocity profiles all over the channel. The main reason for the discrepancies observed with the k–ε realizable and $\overline{v^2}$–f model lies in their underestimation of the turbulent diffusivity, even though the $\overline{v^2}$–f clearly performs better.

These results highlight the difficulties of the RANS models to correctly predict the turbulent momentum transport, and thus energy transport in the near-wall region. This incorrect prediction causes an improper evaluation of the temperature field, in particular in the region near to the wall, where high accuracy is required to correctly predict the convective heat transfer coefficient. Indeed, the eddy diffusivity of heat is directly proportional to the eddy diffusivity of momentum through the turbulent Prandtl number, here considered constant according to the unitary value of the molecular Prandtl number. Only the $\overline{v^2}$–f model can satisfactorily reproduce the local Nusselt number apart from the regions just upstream and downstream of the ribs. Moreover, while the k–ε realizable and k–ω SST models severely underpredict the average Nusselt number, the $\overline{v^2}$–f model is in good agreement with the DNS, which in turn agrees very well with an experimentally determined value.

This systematic comparison between the DNS and RANS simulations highlights the better performance of the $\overline{v^2}$–f model compared to the k–ε realizable for this type of configuration, while the k–ω SST model results to be highly inadequate.

Table 4 Average Nusselt number over the wall

Exper.	DNS	k–ε realizable	k–ω SST	$\overline{v^2}$–f
46	45.29	34.26	32.59	46.66

Nomenclature

c_p = specific heat capacity, J/kg/K
e = rib height, m
f = elliptic relaxation function, m
h = heat transfer coefficient, W/m^2/K $[q_w/(T_w - T_b)]$
H = channel height, m
k = turbulent kinetic energy, m^2/s^2
L_x = streamwise length, m
L_z = spanwise length, m
q_w = wall heat flux, W/m^2
T_b = bulk temperature, K
$T_{b,\mathrm{in}}$ = inlet bulk temperature, K
T_w = wall temperature, K
T_τ = friction temperature, K $[q_w/(\rho c_p u_\tau)]$
u_b = bulk velocity, m/s
u_i = ith velocity component, m/s
u_τ = friction velocity, m/s $(\sqrt{\tau_w/\rho})$
v = wall-normal velocity component, m/s

Nondimensional Numbers

Nu_H = Nusselt number $[(hH)/k]$
Pr = Prandtl number
Re_H = Reynolds number $[(u_b H)/\nu]$
Re_τ = friction Reynolds number $[(u_\tau H/2)/\nu]$

Greek Symbols

α = thermal diffusivity, m^2/s
α_t = turbulent thermal diffusivity, m^2/s
ε = dissipation rate of turbulent kinetic energy, m^2/s^3
λ = thermal conductivity, W/mK
ν = kinematic viscosity, m^2/s
ν_t = turbulent diffusivity, m^2/s
τ_w = wall shear stress, N/m^2
ω = specific rate of dissipation of turbulent kinetic energy, s^{-1}

Operators

$()^+$ = normalization (see text)
$()'$ = fluctuation
$\overline{()}$ = ensemble average value

Abbreviations and Acronyms

CDS = central difference scheme
DNS = direct numerical simulation
FSM = fractional step method
LES = large eddy simulation
RANS = Reynolds-averaged Navier–Stokes
SOU = second-order upwind

References

[1] Casarsa, L., and Arts, T., 2005, "Experimental Investigation of the Aerothermal Performance of a High Blockage Rib-Roughened Cooling Channel," ASME J. Turbomach., **127**(3), pp. 580–588.
[2] Rau, G., Cakan, M., Moeller, D., and Arts, T., 1998, "The Effect of Periodic Ribs on the Local Aerodynamic and Heat Transfer Performance of a Straight Cooling Channel," ASME J. Turbomach., **120**(2), pp. 368–375.
[3] Çakan, M., 2000, "Aero-Thermal Investigation of Fixed Rib-Roughened Cooling Passages," Ph.D. thesis, von Karman Institute for Fluid Dynamics, Université Catholique de Louvain, Leuven, Belgium.
[4] Keshmiri, A., 2012, "Numerical Sensitivity Analysis of 3- and 2-Dimensional Rib-Roughened Channels," Heat Mass Transfer, **48**(7), pp. 1257–1271.
[5] Iacovides, H., and Raisee, M., 1999, "Recent Progress in the Computation of Flow and Heat Transfer in Internal Cooling Passages of Turbine Blades," Int. J. Heat Fluid Flow, **20**(3), pp. 320–328.
[6] Raisee, M., Noursadeghi, A., and Iacovides, H., 2004, "Application of a Non-Linear k-ε Model in Prediction of Convective Heat Transfer Through Ribbed Passages," Int. J. Numer. Methods Heat Fluid Flow, **14**(3), pp. 285–304.
[7] Yap, C., 1987, "Turbulent Heat and Momentum Transfer in Recirculating and Impinging Flows," Ph.D. thesis, Department of Mechanical Engineering, Faculty of Technology, University of Manchester, Manchester, UK.
[8] Ooi, A., Iaccarino, G., Durbin, P., and Behnia, M., 2002, "Reynolds Averaged Simulation of Flow and Heat Transfer in Ribbed Ducts," Int. J. Heat Fluid Flow, **23**(6), pp. 750–757.
[9] Chaube, A., Sahoo, P., and Solanki, S., 2006, "Analysis of Heat Transfer Augmentation and Flow Characteristics Due to Rib Roughness Over Absorber Plate of a Solar Air Heater," Renewable Energy, **31**(3), pp. 317–331.
[10] Tanda, G., 2004, "Heat Transfer in Rectangular Channels With Transverse and V-Shaped Broken Ribs," Int. J. Heat Mass Transfer, **47**(2), pp. 229–243.
[11] Wongcharee, K., Changcharoen, W., and Eiamsa-ard, S., 2011, "Numerical Investigation of Flow Friction and Heat Transfer in a Channel With Various Shaped Ribs Mounted on Two Opposite Ribbed Wall," Int. J. Chem. React. Eng., **9**(1), p. A26.
[12] Kilicaslan, I., and Sarac, I., 1998, "Enhancement of Heat Transfer in Compact Heat Exchanger by Different Type of Rib With Holographic Interferometry," Exp. Therm Fluid Sci., **17**(4), pp. 339–346.
[13] Eiamsa-ard, S., and Promvonge, P., 2008, "Numerical Study on Heat Transfer of Turbulent Channel Flow Over Periodic Grooves," Int. Commun. Heat Mass Transfer, **35**(7), pp. 844–852.
[14] Lorenz, S., Mukomilow, D., and Leiner, W., 1995, "Distribution of the Heat Transfer Coefficient in a Channel With Periodic Transverse Grooves," Exp. Therm Fluid Sci., **11**(3), pp. 234–242.
[15] Luo, D., Leung, C., Chan, T., and Wong, W., 2005, "Flow and Forced-Convection Characteristics of Turbulent Flow Through Parallel Plates With Periodic Transverse Ribs," Numer. Heat Transfer, Part A, **48**(1), pp. 43–58.
[16] Marocco, L., Fustinoni, D., Gramazio, P., and Niro, A., 2011, "First Numerical Results on Forced-Convection Heat Transfer Inside a Rectangular Channel With Straight Ribs on Lower and Upper Walls," XXIX UIT Heat Transfer Conference, pp. 217–222.
[17] Fustinoni, D., Gramazio, P., and Niro, A., 2011, "Heat Transfer Characteristics in Forced Convection Through a Rectangular Channel With Ribbed Surfaces," XXIX UIT Heat Transfer Conference, pp. 63–68.
[18] Marocco, L., Gramazio, P., Fustinoni, D., and Niro, A., 2012, "Numerical Simulation of Forced-Convection Heat Transfer in a Ribbed Channel With High Blockage," XXX UIT Heat Transfer Conference, pp. 259–263.
[19] Miyake, Y., Tsujimoto, K., and Nakaji, M., 2001, "Direct Numerical Simulation of Rough-Wall Heat Transfer in a Turbulent Channel Flow," Int. J. Heat Fluid Flow, **22**(3), pp. 237–244.
[20] Hattori, H., and Nagano, Y., 2012, "Structures and Mechanism of Heat Transfer Phenomena in Turbulent Boundary Layer With Separation and Reattachment Via DNS," Int. J. Heat Fluid Flow, **37**, pp. 81–92.
[21] Rossi, R., 2009, "Direct Numerical Simulation of Scalar Transport Using Unstructured Finite-Volume Schemes," J. Comput. Phys., **228**(5), pp. 1639–1657.
[22] Arts, T., Benocci, C., and Rambaud, P., 2007, "Experimental and Numerical Investigation of Flow and Heat Transfer in a Ribbed Square Duct," 3rd International Symposium on Integrating CFD and Experiments in Aerodynamics, U.S. Air Force Academy, CO, June 20–21, Paper No. ADA515392.
[23] Franco, A., 2013, "Modellazione DNS e RANS della convezione forzata turbolenta in un canale corrugato," Master's thesis, Politecnico di Milano, Milano, Italy (in Italian). [English Translation: "DNS and RANS Modelling of Turbulent Convective Heat Transfer in a Ribbed Channel."]
[24] Patankar, S., Liu, C., and Sparrow, E., 1978, "The Periodic Thermally Developed Regime in Ducts With Streamwise Periodic Wall Temperature or Heat Flux," Int. J. Heat Mass Transfer, **21**(5), pp. 557–566.
[25] Barth, T., and Jespersen, D., 1989, "The Design and Application of Upwind Schemes on Unstructured Meshes," AIAA Paper No. 89-0366.
[26] ANSYS, 2013, "Fluent Manual v.13," ANSYS, Inc., Canonsburg, PA.
[27] Kim, S., and Makarov, B., 2005, "An Implicit Fractional-Step Method for Efficient Transient Simulation of Incompressible Flows," AIAA Paper No. 2005-5253.
[28] Patankar, S. V., 1980, *Numerical Heat Transfer and Fluid Flow*, Hemisphere, Washington, DC.
[29] Kim, J., Moin, P., and Moser, R., 1987, "Turbulence Statistics in Fully Developed Channel Flow at Low Reynolds Number," J. Fluid Mech., **177**, pp. 133–166.
[30] Shih, T.-H., Liou, W. W., Shabbir, A., Yang, Z., and Zhu, J., 1995, "A New k-ε Eddy Viscosity Model for High Reynolds Number Turbulent Flows," Comput. Fluids, **24**(3), pp. 227–238.
[31] Menter, F. R., 1994, "Two-Equation Eddy-Viscosity Turbulence Models for Engineering Applications," AIAA J., **32**(8), pp. 1598–1605.
[32] Durbin, P., 1995, "Separated Flow Computations With the k-ε-$\overline{v^2}$ Model," AIAA J., **33**(4), pp. 659–664.
[33] Wolfshtein, M., 1969, "The Velocity and Temperature Distribution in One-Dimensional Flow With Turbulence Augmentation and Pressure Gradient," Int. J. Heat Mass Transfer, **12**(3), pp. 301–318.
[34] Van Haren, S., 2011, "Testing DNS Capability of OpenFOAM and STAR-CCM+," Master's thesis, Delft University of Technology, Delft, The Netherlands.
[35] Kawamura, H., Ohsaka, K., Abe, H., and Yamamoto, K., 1998, "DNS of Turbulent Heat Transfer in Channel Flow With Low to Medium-High Prandtl Number Fluid," Int. J. Heat Fluid Flow, **19**(5), pp. 482–491.
[36] Wang, L., Salewski, M., and Sundén, B., 2010, "Turbulent Flow in a Ribbed Channel: Flow Structures in the Vicinity of a Rib," Exp. Therm Fluid Sci., **34**(2), pp. 165–176.
[37] Lohász, M., Rambaud, P., and Benocci, C., 2005, "Flow Features in a Fully Developed Ribbed Duct Flow as a Result of LES," *Engineering Turbulence Modelling and Experiments 6*, Elsevier Science B.V., Amsterdam, The Netherlands, pp. 267–276.
[38] Cui, J., Patel, V., and Lin, C., 2003, "Large-Eddy Simulation of Turbulent Flow in a Channel With Rib Roughness," Int. J. Heat Fluid Flow, **24**(3), pp. 372–388.